Shearlet-based Regularization with an Application to Limited Data X-ray Tomography

Zenith Purisha, Imam Solekhudin, Sumardi

***Abstract*—Numerous constrained optimization methods have been suggested to reduce the X-ray dose in computerized tomography. These approaches focus on minimizing a regularizing function, which gauges the deviation from prior knowledge about the imaged object. These approaches focus on minimizing a regularizing function that assesses the lack of consistency of about the object that is being imaged using some prior knowledge. This minimization is conducted under the condition of maintaining a predetermined level of consistency with the detected X-ray attenuation. Total variation (TV) is a frequently explored regularizing function. TV minimization techniques exhibit excellent denoising performance for simple images, yet they lead to the loss of texture information when employed on more complex images. Given that medical imaging frequently involves textured images, utilizing TV may not be advantageous in such scenarios. Alternative studies propose incorporating multi-scale geometric transforms into the regularization function. One recent preference in this regard is the adoption of the shearlets transform. This work presents a proof-of-concept that showcases the application of the discrete shearlets transform as a sparsifying transform in the computed tomography reconstruction solver. Specifically, the regularization term utilized is the ℓ_1-norm of the shearlets coefficients.**

In this work, the algorithm's iterative computation incorporates an operation on the shearlets coefficients. Particularly, the soft-thresholding operator is used with the parameter adaptively chosen. To improve its relevance for biomedical imaging, we propose a desired sparsity level of the thresholding parameter value obtained from a biological object. The effectiveness of the proposed method is assessed using two different types of data: data from chest dataset generated by MATLAB and real data collected from X-ray tomographic measurements of an axial slice of a ladybug.

***Index Terms*—computed tomography, shearlets, sparsity, regularization, adaptive, limited data, biomedical imaging**

I. Introduction

Computed tomography, is widely utilized in diverse sectors including medicine and industry. In a standard computed tomography imaging, the scanner detectors capture projections from various angles. These projections are later processed to generate a computed tomography image that approximates the internal distribution of the object's X-ray attenuation [1]. Recently, there has been a growing interest in minimizing X-ray dosage in computed tomography scans. While there have been suggestions to achieve this by reducing the current in the X-ray emitting hardware or shortening the duration of the X-ray pulse, the approach that has received the most attention involves a substantial decrease in the number of X-ray projections. The schemes lead to a degradation of reconstruction image quality, especially when employing the filtered back-projection reconstruction algorithm, which is the most widely used method for generating computed tomography images. As a result, extensive research has been dedicated to employing constrained optimization methods.

A mathematical model in a variational form to reconstruct images is carried out in this work. Previous studies extensively delved into various well-known techniques employing sparsity-based inversion with a particular focus on under-sampled computed tomography explored in [2], [3]. In our investigation, shearlets are considered as the chosen sparsifying transform [4]. Theoretically, shearlets exhibit superior directional sensitivity and avoid the undesirable staircasing effect.

Consider the mathematical as follows

$$\boldsymbol{f}_{\mathrm{S}} = \underset{\boldsymbol{f}\in\mathbb{R}^{N^2},\, \boldsymbol{f}\geq 0}{\operatorname{argmin}} \left\{ \frac{1}{2}\|\mathbf{R}\boldsymbol{f} - \boldsymbol{m}\|_2^2 + \tau\|\mathbf{S}\boldsymbol{f}\|_1 \right\}. \quad (1)$$

In detail, $\mathbf{R}$ is a measurement matrix, $\boldsymbol{f}$ is an object of interest, $\boldsymbol{m}$ is the measured data and $\mathbf{S}$ is a shearlets matrix. Parameter τ is used as a regularization parameter.

The idea to control the regularization parameter is carried out in this work to solve the problem 1. Specifically, the algorithm determines the parameter τ automatically to obtain a specified level of sparsity for the shearlets coefficients [5]. Both artificial and real data are used to conduct the numerical experiments. To support the rationale presented in this work, an axial slice of a ladybug is measured for the real data. While the under-sampled computed tomography problem has been a subject of ongoing interest, the application of shearlets with an automatically chosen thresholding parameter (τ) for biological tissue images is a novel contribution. Additionally, the introduction of prior information regarding the desired sparsity level based on biological matter is a new concept. The reconstructed images using the algorithm are compared with those using the filtered back-projection [6], [7], [8].

The model of the computed tomography problem and the algorithm are addressed in Section III and Section V. The image reconstructions and the discussions are reported in Section VII and Section VIII.

II. 2D shearlets

The key concepts related to shearlets are discussed in this section. Shearlets are designed to enable directional representation systems for multidimensional data [9], [10]. A key feature of shearlets is their capacity to manage directional orientations via the shearing parameter. Images with anisotropic singularities can be detected well by the element of shearlets system, namely various scales, locations, and orientations [11]. It is important to highlight that the

Manuscript received March 28, 2024; revised September 9, 2024.

Zenith Purisha is an Assistant Professor at the Department of Mathematics, Universitas Gadjah Mada, Indonesia. E-mail: zenith.purisha@ugm.ac.id

Imam Solekhudin is a Professor at the Department of Mathematics, Universitas Gadjah Mada, Indonesia. E-mail: imams@ugm.ac.id

Sumardi is an Associate Professor at the Department of Mathematics, Universitas Gadjah Mada, Indonesia. E-mail: mardimath@ugm.ac.id

shearlets system operates as a frame rather than a basis. To enhance readability, we concentrate on presenting the general concepts and encourage interested readers to the cited literature for more details and precise formulations. The following definition specifies a class of functions to model the image containing anisotropic singularities.

Definition II.1. The *class* $\mathscr{E}^2(\mathbb{R}^d)$ *of cartoon-like image* is the set of functions $f : \mathbb{R}^2 \to \mathbb{C}$ of the form

$$f = f_0 + f_1\chi_B, \tag{2}$$

being $B \subset [0,1]^2$ is a set with ∂B being a closed C^2-curve with bounded curvature and $f_i \in C^2(\mathbb{R}^2)$ are functions with $\text{supp} f_0 \subset [0,1]^2$ and $\|f_i\|_{C^2} \leq 1$ for each $i = 0, 1$.

In the following, a discrete shearlets system is derived. It allows us to encode anisotropic features in the digital realm. The *discrete sheartets system* associated with $\xi \in L^2(\mathbb{R}^2)$ is defined by

$$\{\xi_{j,k,m} = 2^{3/4}\xi(S_k A_{2^j} \cdot -m) : j, k \in \mathbb{Z}, m \in \mathbb{Z}^2\}, \tag{3}$$

where
$S_k = \begin{bmatrix} 1 & k \\ 0 & 1 \end{bmatrix}$, is a *shearing matrix*,
$A_{2^j} = \begin{bmatrix} 2^j & 0 \\ 0 & 2^{j/2} \end{bmatrix}$, is *a parabolic scaling matrix* and being j is the scale index, k is the orientation index and m is the position index.

Furthermore, the *discrete shearlet transform* is defined as the mapping

$$L^2(\mathbb{R}^2) \ni f \to \mathcal{SH}(f) = \langle f, \xi_{j,k,m}\rangle, \quad (j,k,m) \in \mathbb{Z}\times\mathbb{Z}\times\mathbb{Z}^2. \tag{4}$$

The cone-adapted two-dimensional discrete shearlets systems are introduced by partitioning the frequency plane into four cones to avoid the shear parameters to become excessively large.

Definition II.2. Let $\phi, \xi, \tilde{\xi} \in L^2(\mathbb{R}^2)$. The cone-adapted discrete shearlets system $SH(\phi, \xi, \tilde{\xi}; c)$ is defined by

$$SH(\phi, \xi, \tilde{\xi}; c) = \Phi(\phi; c_1) \cup \Xi(\xi; c) \cup \tilde{\Xi}(\tilde{\xi}; c)$$

where

$$\begin{aligned}
\Phi(\phi; c_1) &= \{\phi_m = \phi(\cdot - c_1 m) : m \in \mathbb{Z}^2\}, \\
\Xi(\psi; c) &= \{\xi_{j,k,m} = 2^{\frac{3}{4}j}\xi(S_k A_{2^j} \cdot -M_c m) : \\
&\qquad j \geq 0, |k| \leq \lceil 2^{j/2}\rceil, m \in \mathbb{Z}^2)\}, \\
\Xi(\xi; c) &= \{\xi_{j,k,m} = 2^{\frac{3}{4}j}\xi(S_k A_{2^j} \cdot -M_c m) : \\
&\qquad j \geq 0, |k| \leq \lceil 2^{j/2}\rceil, m \in \mathbb{Z}^2)\}, \\
\tilde{\Xi}(\xi; c) &= \{\tilde{\xi}_{j,k,m} = 2^{\frac{3}{4}j}\tilde{\xi}(S_k^T A_{2^j} \cdot \\
&\quad -\tilde{M}_c m) : j \geq 0, |k| \leq \lceil 2^{j/2}\rceil, m \in \mathbb{Z}^2)\},
\end{aligned}$$

with $c = (c_1, c_2) \in (\mathbb{R}_+)^2$, $M_c = \begin{bmatrix} c_1 & 0 \\ 0 & c_2 \end{bmatrix}$ and $\tilde{M}_c = \begin{bmatrix} c_2 & 0 \\ 0 & c_1 \end{bmatrix}$.

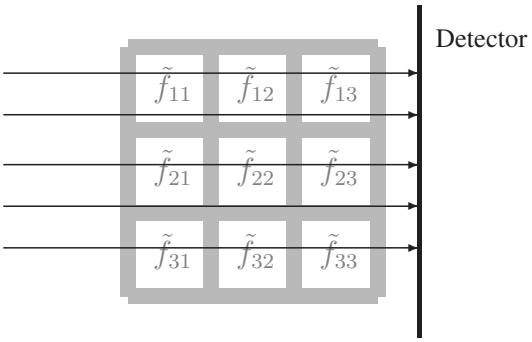

Fig. 1. An illustration of the measurement model.

III. Variational model

In computed tomography, a detector captures incoming X-ray photons, and the measurement data are collected by taking into account the intensity reductions of X-rays across various projections. In this context, the available projections are limited.

Let $\Omega \subset \mathbb{R}^2$ and $f : \Omega \subset \mathbb{R}^2 \to \mathbb{R}_+$. The object of interest is an unknown non-negative attenuation coefficient function, $f(x_1, x_2)$, which represents an inner structure of the object at point (x_1, x_2). The beam of X-ray L denotes a straight line carrying intensity that passes through the object. The measurement data is characterized by a line integral of $f(x_1, x_2)$, and the object is reconstructed based on this integral.

In practice, $f(x)$ is expressed by a matrix $\boldsymbol{f} = [\tilde{f}_{ij}] \in \mathbb{R}^{N\times N}$ (see Figure 1).

The mathematical model of the problem is as follows

$$\int_L f(x)\, ds = \sum_{i=1}^{N}\sum_{j=1}^{N} a_{ij}\tilde{f}_{ij}, \tag{5}$$

In detail, the X-ray beam L passes through a_{ij} where index-ij associated with the pixel (i, j). The Equation 5 is then formulated as

$$\boldsymbol{m} = \mathbf{R}\boldsymbol{f}, \tag{6}$$

where $\mathbf{R} = [a_{ij}] \in \mathbb{R}^{M\times N^2}$ is the measurement matrix and $\boldsymbol{m} \in \mathbb{R}^M$ is the vector of the measurement data.

It is widely acknowledged that in the case of undersampled data, the linear system in Equation 6 gives rise to a discrete inverse problem that is highly ill-posed. Therefore, regularization is required to address this problem. Consider a variational functional of the form

$$\underset{\boldsymbol{f}\in\mathbb{R}^{N^2},\, \boldsymbol{f}\geq 0}{\text{argmin}} \ \frac{1}{2}\|\mathbf{R}\boldsymbol{f} - \boldsymbol{m}\|_2^2 + \tau\|\mathbf{S}\boldsymbol{f}\|_1 \tag{7}$$

where τ is the regularization parameter, $\mathbf{S}$ is the shearlets transform in the form of matrix. We take into account the prior knowledge of $\boldsymbol{f}$, which quantifies the incoming photons without generating new photons by enforcing the non-negativity constraint for $\boldsymbol{f}$.

IV. Adaptive thresholding parameter τ

We consider to alter the parameter τ in the problem 7 adaptively using the concept of proportional-integral-derivative (PID) controllers [12], [13], [14], [15]. Given a vector of shearlets coefficient $\{w_i\} \in \mathbb{R}^{N^2}$ for $1 \leq i \leq N^2$. The shearlets coefficients that larger than ν is defined by

$$C_\nu = \{w_i | |w_i| > \nu\}.$$

The goal is to find a value of ν such that the shearlets give the best approximation for a given image. Let us write the problem as follows

$$\nu^\star = \arg\min_{\nu} \|\boldsymbol{f}_{pr} - \mathbf{S}^T(C_\nu)\|,$$

where $\boldsymbol{f}_{pr}$ is an object that similar to the target. The desired sparsity level of shearlets from the target is given by

$$C_{pr} = \dim\{w_i | |w_i| > \nu^\star\}. \tag{8}$$

Let β equals to the mean of the absolute values of the shearlets coefficients, then the parameter τ alters as follows:

$$\tau_{(k+1)} = \tau_{(k)} + \beta(C_{(k)} - C_{pr}),$$

where C_k is the degree of sparsity at k^{th} iteration.

V. Controlled Shearlets Domain Sparsity Algorithm

The idea implementing the automatic chosen the regularization parameter τ in the shearlets coefficient domain is considered in this work [16], [17], [5]. The parameter τ is chosen automatically using the algorithm outlined in Algorithm 1. The computation to minimize the problem (1) uses a primal-dual method used in [18] as follows:

$$\begin{aligned}
\boldsymbol{m}_{(k+1)} &= \mathbb{P}_C\Big(\boldsymbol{f}_{(k)} - \mu\nabla g(\boldsymbol{f}_{(k)}) - \lambda\mathbf{S}^T\boldsymbol{w}_{(k)}\Big) \\
\boldsymbol{w}_{(k+1)} &= \Big(I - \mathcal{T}_\tau\Big)\Big(\mathbf{S}\boldsymbol{m}_{(k+1)} + \boldsymbol{w}_{(k)}\Big) \\
\boldsymbol{f}_{(k+1)} &= \mathbb{P}_C\Big(\boldsymbol{f}_{(k)} - \mu\nabla g(\boldsymbol{f}_{(k)}) - \lambda\mathbf{S}\mathbf{S}^T\boldsymbol{w}_{(k+1)}\Big)
\end{aligned} \tag{9}$$

where μ and λ are positive parameters, here $0 < \mu < 2/\mu_{\text{l}}$ where μ_{l} is the Lipschitz constant for $g(\boldsymbol{f})$, $g(\boldsymbol{f}) = \frac{1}{2}\|\mathbf{R}\boldsymbol{f} - \boldsymbol{m}\|_2^2$ and the operator $\mathcal{T}$ reads as

$$\mathcal{T}_\tau(x) = \begin{cases} x + \frac{\tau}{2} & \text{for } x \leq -\frac{\tau}{2} \\ 0 & \text{for } |x| < \frac{\tau}{2} \\ x - \frac{\tau}{2} & \text{for } x \geq -\frac{\tau}{2}. \end{cases} \tag{10}$$

In detail, let $\lambda_{\max}$ is the maximum eigenvalue, $0 < \lambda < 1/\lambda_{\max}(\mathbf{S}\mathbf{S}^T)$. Notation $\mathbb{P}_C$ represents the Euclidean projection on C where $C = \mathbb{R}_+^{N^2}$.

VI. Numerical Experiments

In this work, two types of measurement data from artificial phantom and real target are used. The data are acquired for two different types of data (see section VI-A) using thirty and fifteen projection view of angles. The computational implementation is conducted using Matlab 9.11 (R2021b) on an Apple M1 with 8GB of CPU memory. Spot–A Linear-Operator Toolbox [19] is used to generate the shearlets matrix $\mathbf{S}$. The number of scales is 2. The stopping criterion is controlled by parameters ε_1 and ε_2 and both are set equal to 10^{-2}.

Algorithm 1 The controlled shearlets domain sparsity algorithm

Inputs: measurement data $\boldsymbol{m}$, measurement matrix $\mathbf{R}$, parameters τ, $\lambda > 0$ to ensure convergence, *a priori* degree of sparsity C_{pr}, initial thresholding parameter $\tau_{(0)}$, maximum number of iterations $N_{\max} > 0$, parameter tolerances $\varepsilon_1, \varepsilon_2 > 0$ for the stopping rule, and control stepsize $\beta > 0$.
$\boldsymbol{f}_{(0)} = \mathbf{0}$, $k = 0$, $e = 1$, and $C_{(0)} = 1$
while $k < N_{\max}$ and $|e| \geq \varepsilon_1$ or $\varepsilon \geq \varepsilon_2$ **do**
  $e = C_{(i)} - C_{pr}$
  if $\text{sign}(e_{(k+1)}) \neq \text{sign}(e_{(k)})$ **then**
    $\beta = \beta(1 - |e_{(k+1)} - e_{(k)}|)$
  $\tau_{(k+1)} = \max\{0, \tau_{(k)} + \beta e\}$
  $\boldsymbol{m}_{(k+1)} = \max\{0, \boldsymbol{f}_{(k)} - \gamma\nabla g(\boldsymbol{f}_{(k)}) - \lambda\mathbf{S}^T\boldsymbol{w}_{(k)}\}$
  $\boldsymbol{w}_{(k+1)} = (I - \mathcal{T}_{\tau_{(k)}})(\mathbf{S}\boldsymbol{m}_{(k+1)} + \boldsymbol{w}_{(k)})$
  $\boldsymbol{f}_{(k+1)} = \max\{0, \boldsymbol{f}_{(k)} - \gamma\nabla g(\boldsymbol{f}_{(k)}) - \lambda\mathbf{S}^T\boldsymbol{w}_{(k+1)}\}$
  $C_{(k+1)} = \frac{1}{N^2}\dim\{\mathbf{S}\boldsymbol{f}_{(k+1)} | \text{abs}(\mathbf{S}\boldsymbol{f}_{(k+1)}) > 10^{-6}\}$
  $\varepsilon = \|\boldsymbol{f}_{(k+1)} - \boldsymbol{f}_{(k)}\|_2 / \|\boldsymbol{f}_{(k+1)}\|_2$
  $k := k + 1$

A. Experimental data

A chest dataset is generated with Matlab (see Figure 2) as an artifical phantom and it is used to produce artificial data. The phantom size is 128×128. The artificial data is simulated using noisy measurements.

Fig. 2. The artificial chest phantom used as a ground truth.

For the real data, X-ray projections of an axial slide a ladybug (see Figure 3) that contains biological matters are acquired. In detail, the dataset is available at here and the geometry setup is documented in [20].

B. Numerical results

This section presents numerical results of X-ray tomographic image reconstructions using a controlled shearlets domain sparsity as a proposed method. Two datasets: artificial data and real data as provided in VI-A are tested.

As discussed in Section IV, the proposed method implements the Algorithm 1. Matrix $\mathbf{R}$ contains the measurement model of 5. Data $\boldsymbol{m}$ is obtained using measured data in VI-A. The parameter $\tau = 1$ and the parameter $\lambda = 0.99$ to ensure the convergence. The reconstructions using the controlled

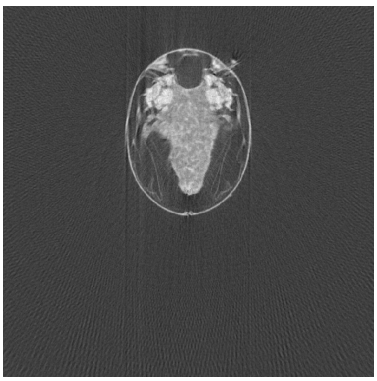

Fig. 3. Th reconstructed image of the axial slice of ladybug using filtered back-projection from complete projections.

TABLE I
COMPARISON OF RECONSTRUCTION METHODS FOR 30 PROJECTIONS

Methods	Relative Error	PSNR	SSIM
Filtered back-projection	0.252	52.789	0.992
Proposed approach	0.208	54.45	0.996

shearlets domain sparsity method are reported in Figure 7(b) and Figure 8(b).

Figure 4(a) presents the reconstructed image of chest phantom by employing filtered back-projection method for 30 projections data and Figure 4(b) presents the reconstructed image from the same data using the controlled shearlets domain sparsity method. The average quality measures on the reconstructed images are reported in Table I. Using the proposed algorithm, to reconstruct the images, the computation requires 126 iterations and takes 45 seconds.

The reconstructed images of the axial slice of the ladybug using the filtered back-projection and the proposed method using 30 projections are shown in Figure 7. Figure 8 shows the 15-projections reconstruction. The filtered back-projection reconstructions from complete projections data are presented as a ground truth for a qualitative analysis. The reconstructed images of the axial slice of the ladybug using the filtered back-projection are shown in Figure 7(a) and Figure 8(a).

In this work, the $\boldsymbol{f}_{pr}$ is the reconstructed image of the axial slice of the ladybug using filtered back-projection using complete projections, namely 360 projections.. The shearlets sparsity levels as the iteration progresses are plotted in the Figure 6 and Figure 9. According to 8, the sparsity level C_{pr} equals to 60%. The stopping rule ε_1 is set to be 10^{-2}. it is shown that the level of sparsity converges to the desired sparsity level C_{pr}. The computational complexity of the controlled shearlets domain sparsity algorithm is higher than the filtered back-projection method. The computation time is reported in Table II.

VII. DISCUSSION

This work presents a method for reconstructing computed tomography images from under-sampled measurement data through the application of an adaptive shearlets domain sparsity algorithm. Our approach incorporates the use of shearlets. We evaluate our proposed method using both

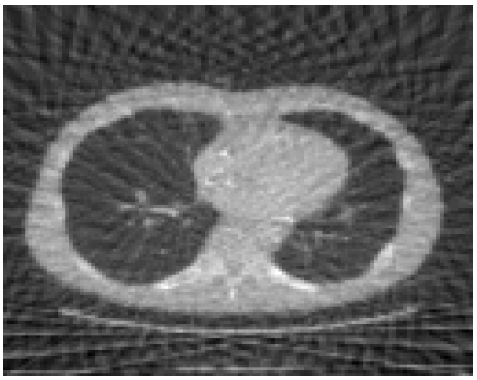

(a)

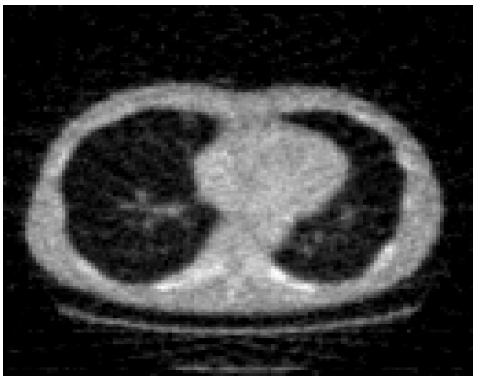

(b)

Fig. 4. (a) The reconstructed images of the chest phantom using filtered back-projection and (b) controlled shearlets domain sparsity algorithm (b) from 30 projections.

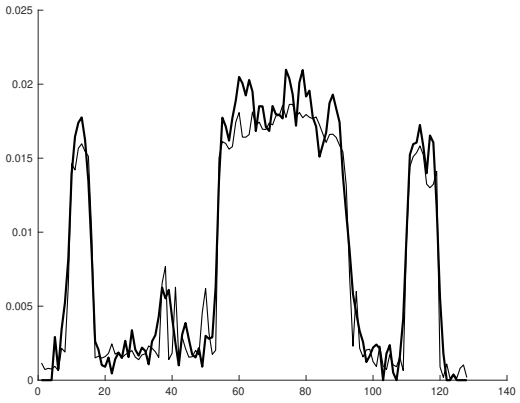

Fig. 5. Line profiles of Figure 2 (thin line) and Figure 4(b) (thick line)

TABLE II
COMPUTATION TIME (IN SECONDS)

Methods	30 projections	15 projections
FBP	1.4	0.17
Proposed approach	64	96

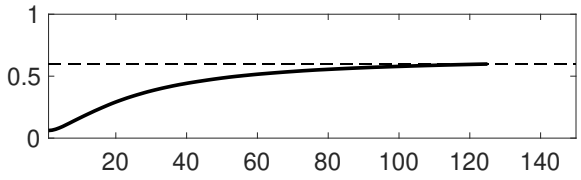

Fig. 6. The nonzero shearlets coefficients of the reconstruction of the chest phantom as the iteration progresses for 30 projections.

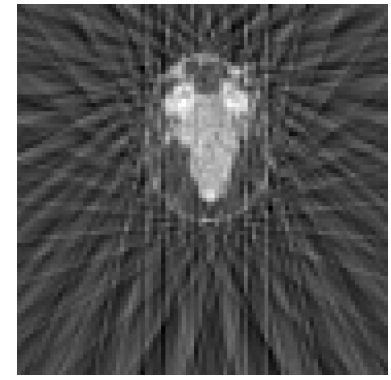

(a)

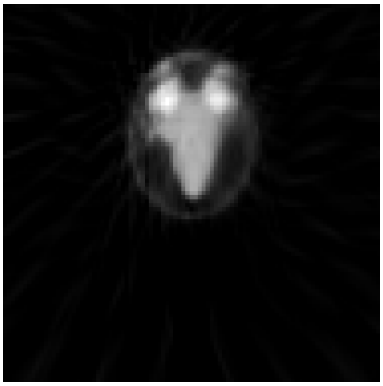

(b)

Fig. 7. (a) The reconstructed images of the axial slice of the ladybug using filtered back-projection and (b) controlled shearlets domain sparsity algorithm from 30 projections.

artificial chest data and real data as detailed in VI-A. The projections are quite sparse, consisting of fifteen and thirty projections. The mathematical model is framed as an ℓ^1-minimization problem, employing a sparsifying shearlets transform as ℓ^1-regularization in the penalty term. To solve this, the parameter in the regularization term is selected automatically.

The reconstructed images of the chest phantom using filtered back-projection from 30 projections shows artifacts in almost every region. In contrast, employing the proposed

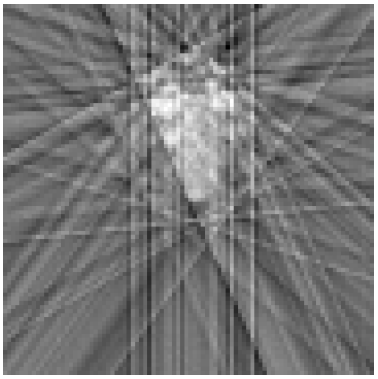

(a)

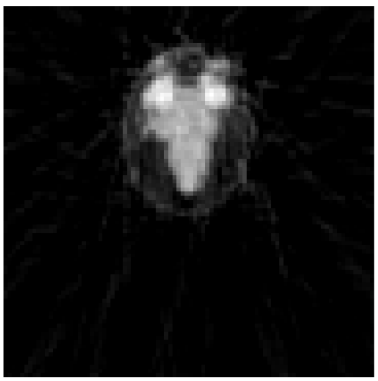

(b)

Fig. 8. (a) The reconstructed images of the the axial slice of the ladybug using filtered back-projection and (b) controlled shearlets domain sparsity algorithm (b) from 15 projections.

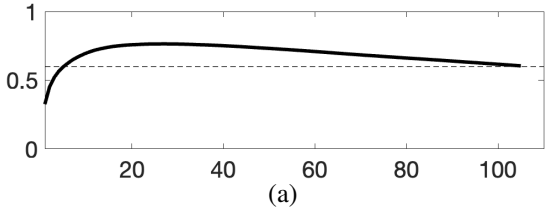

(a)

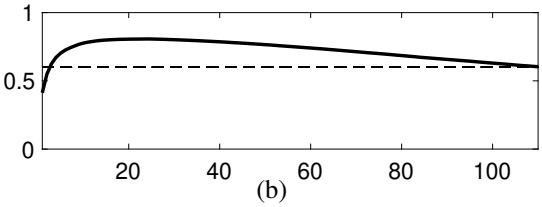

(b)

Fig. 9. The nonzero shearlets coefficients of the reconstruction for the axial slice of the ladybug as the iteration progresses using (a) 30 projections and (b) 15 projections.

method for chest reconstruction with the same number of projections effectively recovers singularities, capturing edges of the inner structures of the object as well as the background of the object. The resulting reconstructed image is less predominantly characterized by artifacts.

Image reconstructions of filtered back-projection are significantly dominated by artifacts. Additionally, the lack of a non-negativity constraint in the filtered back-projection algorithm leads to poor representation of pixels with zero or very low attenuation values. In contrast, the artifacts in the image reconstructions of the proposed method are reduced. A closer look indicates that the non-negativity constraint improves the quality of the reconstructions. For instance, in the filtered back-projection reconstruction, a thin, elongated line in the lower chest area is covered by line artifacts, primarily due to angular sub-sampling. However, with the proposed method, this thin line is restored well.

A line profile of the reconstruction using the proposed method using 15 projections is reported in Figure 5. It shows that the profile follows the shape of the profile of the ground truth image with a small difference in the intensity value.

In real data, the axial slice of the ladybug is reconstructed using 15 and 30 projections. A greater presence of artifacts is shown in the filtered back-projection reconstruction compared to the controlled shearlets domain sparsity strategy. Particularly, the reconstructions from the proposed method capture finer details with fewer artifacts. Additionally, because the non-negativity penalty is carried out in the model, the reconstruction image is enhanced. Dominant features of the ladybug also accurately represented.

VIII. Conclusion

Reconstructed computed tomography images of the biological object is presented in this paper. The reconstruction uses under-sampled measurement data through the application of an adaptive shearlets domain sparsity algorithm. The results indicate that images reconstructed from artificial data using the proposed method exhibit better quality than those generated by the filtered back-projection algorithm. We evaluate image quality using metrics such as PSNR, SSIM, and relative error.

Reconstructed images of the axial of the ladybug using the controlled shearlets domain sparsity effectively captures the details for the features of it by leveraging the information of the desired sparsity level. Furthermore, this value could be considered to obtain X-ray tomographic reconstructions from various biological object. Importantly, the algorithm and its procedures could be extended to a wide range of other tomographic applications.

References

[1] T. M. Buzug, "Computed tomography," in *Springer handbook of medical technology*. Springer, 2011, pp. 311–342.

[2] G. R. Easley, D. Labate, and F. Colonna, "Shearlet-based total variation diffusion for denoising," *IEEE Transactions on Image processing*, vol. 18, no. 2, pp. 260–268, 2008.

[3] S. Loock and G. Plonka, "Phase retrieval for fresnel measurements using a shearlet sparsity constraint," *Inverse Problems*, vol. 30, no. 5, p. 055005, 2014.

[4] T. A. Bubba, G. Kutyniok, M. Lassas, M. März, W. Samek, S. Siltanen, and V. Srinivasan, "Learning the invisible: A hybrid deep learning-shearlet framework for limited angle computed tomography," *Inverse Problems*, vol. 35, no. 6, p. 064002, 2019.

[5] Z. Purisha, "Computed tomography reconstruction from undersampled data: An application to biomedical imaging." *IAENG International Journal of Applied Mathematics*, vol. 54, no. 1, 2024.

[6] A. C. Kak and M. Slaney, *Principles of computerized tomographic imaging*. SIAM, 2001.

[7] J. S. Jørgensen and E. Y. Sidky, "How little data is enough? phase-diagram analysis of sparsity-regularized x-ray computed tomography," *Philosophical Transactions of the Royal Society A: Mathematical, Physical and Engineering Sciences*, vol. 373, no. 2043, p. 20140387, 2015.

[8] E. Y. Sidky and X. Pan, "Image reconstruction in circular cone-beam computed tomography by constrained, total-variation minimization," *Physics in Medicine & Biology*, vol. 53, no. 17, p. 4777, 2008.

[9] K. Guo, G. Kutyniok, and D. Labate, "Sparse multidimensional representations using anisotropic dilation and shear operators," *Wavelets and splines*, vol. 14, pp. 189–201, 2006.

[10] G. Kutyniok, V. Mehrmann, and P. C. Petersen, "Regularization and numerical solution of the inverse scattering problem using shearlet frames," *Journal of Inverse and Ill-posed Problems*, vol. 25, no. 3, pp. 287–309, 2017.

[11] G. Kutyniok and D. Labate, *Shearlets: Multiscale analysis for multivariate data*. Springer Science & Business Media, 2012.

[12] K. J. Åström and T. Hägglund, *PID controllers: theory, design, and tuning*. ISA Research Triangle Park, NC, 1995.

[13] S. Parvez and Z. Gao, "A wavelet-based multiresolution pid controller," *IEEE Transactions on Industry Applications*, vol. 41, no. 2, pp. 537–543, 2005.

[14] M. Araki, "Pid control," *Control Systems, Robotics and Automation: System Analysis and Control: Classical Approaches II, Unbehauen, H.(Ed.). EOLSS Publishers Co. Ltd., Oxford, UK., ISBN-13: 9781848265912*, pp. 58–79, 2009.

[15] J. Sun, W. Tian, H. Che, S. Sun, S. Gao, L. Xu, and W. Yang, "Proportional–integral controller modified landweber iterative method for image reconstruction in electrical capacitance tomography," *IEEE Sensors Journal*, vol. 19, no. 19, pp. 8790–8802, 2019.

[16] Z. Purisha, J. Rimpeläinen, T. Bubba, and S. Siltanen, "Controlled wavelet domain sparsity for x-ray tomography," *Measurement Science and Technology*, vol. 29, no. 1, p. 014002, 2017.

[17] Z. Purisha, S. S. Karhula, J. H. Ketola, J. Rimpeläinen, M. T. Nieminen, S. Saarakkala, H. Kröger, and S. Siltanen, "An automatic regularization method: An application for 3-d x-ray micro-ct reconstruction using sparse data," *IEEE transactions on medical imaging*, vol. 38, no. 2, pp. 417–425, 2018.

[18] P. Chen, J. Huang, and X. Zhang, "A primal-dual fixed point algorithm for minimization of the sum of three convex separable functions," *Fixed Point Theory and Applications*, vol. 2016, no. 1, p. 54, 2016.

[19] E. Van den Berg and M. Friedlander, "Spot – a linear-operator toolbox," http://www.cs.ubc.ca/labs/scl/spot/, accessed: 2013-02-08.

[20] J. Juurakko, Z. Purisha, and S. Särkkä, "Dynamic 3d tomographic x-ray data of ladybug," 2019. [Online]. Available: https://arxiv.org/abs/1908.08782